TITLE

Coupled proliferation and apoptosis maintain the rapid turnover of microglia in the adult brain

AUTHORS

Katharine Askew[1], Kaizhen Li[2], Adrian Olmos-Alonso[1], Fernando Garcia-Moreno[3], Yajie Liang[2], Philippa Richardson[1], Tom Tipton[4], Mark A. Chapman[1], Kristoffer Riecken[5], Sol Beccari[6], Amanda Sierra[6], Zoltán Molnár[3], Mark S. Cragg[4], Olga Garaschuk[2], V. Hugh Perry[1], Diego Gomez-Nicola*[1]

1. Biological Sciences, University of Southampton, UK
2. Institute of Physiology II, University of Tübingen, Germany
3. Department of Physiology, Anatomy and Genetics, University of Oxford, UK
4. Antibody and Vaccine Group, Cancer Sciences Unit, University of Southampton, UK
5. Research Dept. Cell and Gene Therapy, University Medical Center Hamburg-Eppendorf, Germany
6. Achucarro Basque Center for Neuroscience, Ikerbasque Foundation, University of the Basque Country (UPV/EHU), Spain.

*__LEAD CONTACT__

Diego Gomez-Nicola, PhD

Biological Sciences. University of Southampton

South Lab&Path Block. Mail Point 840, LD80C. Southampton General Hospital. Tremona Road. SO166YD.

Southampton, United Kingdom.

e-mail: d.gomez-nicola@soton.ac.uk

RUNNING TITLE: Dynamics of microglia in the adult brain

SUMMARY

Microglia play key roles in brain development, homeostasis and function and it is widely assumed that the adult population is long-lived and maintained by self-renewal. However, the precise temporal and spatial dynamics of the microglial population are unknown. We show in mice and humans that the turnover of microglia is remarkably fast, allowing the whole population to be renewed several times during a lifetime. The number of microglial cells remains steady from late postnatal stages until ageing, and is maintained by the spatial and temporal coupling of proliferation and apoptosis, as evidenced by pulse-chase studies, chronic in vivo imaging of microglia and the use of mouse models of dysregulated apoptosis. Our results reveal that the microglial population is constantly and rapidly remodelled, opening new avenues into the understanding of their roles in the maintenance of brain homeostasis.

INTRODUCTION

Microglial cells are the brain's resident innate immune cells, with proposed key roles in immune to brain communication and the control of inflammation in brain disease (Gomez-Nicola and Perry, 2015), the developmental control of neurogenesis (Cunningham et al., 2013), wiring (Squarzoni et al., 2014) and synaptic pruning(Paolicelli et al., 2011), the monitoring of synaptic activity(Wake et al., 2009) and the regulation of adult neurogenesis (Sierra et al., 2010). Microglia account for 5-12% of the total number of glial cells in the mouse brain (Lawson et al., 1990) and 0.5-16.6% of the total number of cells in the human brain (Mittelbronn et al., 2001) depending on the region studied.

Microglia are derived from the yolk sac at E8.5 (Ginhoux et al., 2010), a lineage distinct from the majority of other tissue-resident macrophages (Hoeffel et al., 2015) and acquire their definitive local density soon after birth, after a wave of microglial proliferation at early postnatal stages (Nikodemova et al., 2015). However, it is unclear if proliferation alone can account for the rapid increase in microglial numbers and suggests the possibility of additional recruitment and differentiation from blood-derived monocytes perinatally (Ginhoux et al., 2013), although the contribution of monocytes have not been observed in fate mapping studies (Hoeffel et al., 2015, Sheng et al., 2015).

In the adult, it has been suggested that the microglial population is long-lived and maintained by self-renewal (Lawson et al., 1992), although the dynamics of the microglial population in the adult brain are largely unknown. However, evidence arising from manipulations of the numbers of resident microglial cells highlights that this population can be rapidly reconstituted by the proliferation of resident cells after genetic ablation using the Cx3cr1CreER-based system (Bruttger et al., 2015), pharmacological elimination (Elmore et al., 2014), or by infiltrating monocytes after

the death of microglia induced using the CD11b-TK system (Varvel et al., 2012). Microglia are rarely replaced by bone-marrow (BM) derived progenitors in health or disease (Gomez-Nicola and Perry, 2015). These observations suggest that microglia resemble the behaviour of other tissue-resident macrophage populations, like lung or BM macrophages, which are maintained by self-renewal in the steady state(Hashimoto et al., 2013). Although these studies suggest that microglia are a dynamic population and give some clues about the molecular determinants of the re-population response, we do not know the rules governing the homeostatic maintenance of microglia during an organism's lifetime.

In this study we show that the adult microglial population is formed without a contribution from circulating progenitors. We show that in the adult mouse and human brain, microglia display a high proliferation rate that accounts for several rounds of renewal of the whole population during the organism's lifetime. This proliferation is temporally and spatially coupled to intrinsic apoptosis, resulting in the maintenance of a relatively steady number of cells from early postnatal stages through to ageing. Our results reveal a highly dynamic but tightly regulated control of microglial cell numbers, opening new avenues into the understanding of the functions of microglia in the healthy and diseased brain.

RESULTS

A perinatal wave of infiltrating monocytes does not contribute to the adult microglial population

Although recent evidence supports the concept that the adult microglial population is generated from yolk sac emigrants (Ginhoux et al., 2010), followed by a wave of microglial proliferation (Nikodemova et al., 2015), it is unclear if this, alone, accounts for the total increase in microglial cell numbers. Contrasting reports described the infiltration of blood-derived monocytes into the brain at perinatal stages (Alliot et al., 1999, Tambuyzer et al., 2009), although monocytes have been shown not to contribute to the adult microglial population (Hoeffel et al., 2015, Sheng et al., 2015). To address this question, we used a novel approach to label and track hematopoietic cells during embryonic development, based on the *in utero* intra-liver delivery of lentiviral LeGO vectors driving the expression of the fluorescent protein Venus at E14, a stage when the liver is the main hematopoietic organ (Fig. 1a). This method allows rapid, selective and minimally invasive tracing of cells from the hematopoietic lineage, and further analysis in target organs. Intra-liver tracing at E14 and subsequent analysis of the brain from P0 onwards allowed the visualization of waves of infiltrating monocytes ($Venus^+$), acquiring migratory (bipolar, elongated; 87.9% of all $Venus^+$ cells at P3) or ramified (multiple radially orientated processes; 12.0% of all $Venus^+$ cells at P3) phenotypes within the brain's parenchyma (Fig. 1b, 1c). The visualization of the differentiation of $Venus^+$ cells into ramified Iba1-expressing morphologies supported the use of this tracking method for long-term purposes, as the expression of the Venus transgene was not affected by phenotypic changes with postnatal age (Fig. 1c). $Venus^+$ cells were not found in the perivascular space of the blood vessels or in the meninges. This, together with the morphologies observed in in Fig. 1c, supports that $Venus^+$ cells infiltrate the parenchyma proper. The

quantification of the total Venus$^+$ cells (ramified+migratory; Fig. 1b, 1c) evidenced the time-course of infiltration (Fig. 1d, 1e). This wave of infiltration was coincident in time with the expansion of the resident microglial population (Iba1$^+$Venus$^-$) followed by further refinement (Fig. 1d), in accord with previously reported data (Nikodemova et al., 2015). After a peak of infiltration at P3, the infiltrated monocytes were found to radically decrease in number until only rare cells survive in the adult brain (Fig. 1e). These cells were not observed when vectors were delivered to the amniotic sac, supporting the specificity of the intra-liver approach. Intra-liver injections were comparable in different litters, as evidenced by a comparable degree of labelling of Kupffer cells and hepatocytes in the liver (Fig. 1f), preserved over time. Venus$^+$ cells in the brain parenchyma were identified at P3 to be CD206^{low}, when compared with choroid plexus or perivascular macrophages (Fig. 1g), and GFAP$^-$Olig2$^-$NG2$^-$ (Fig. 1h), supporting their monocytic lineage. Venus$^+$ cells were also defined as non-proliferative cells (Venus$^+$BrdU$^-$) in the different regions analysed (Fig. 1i).

The analysis of cell death in the Venus$^+$ population revealed an apoptotic response from P3, as identified by the expression of cleaved caspase-3 or chromatin condensation (non-significant difference between activated Caspase-3$^+$ cells vs cells with condensed nuclei stained with DAPI)(Fig. 1j). We found that at P3 1.83% (condensed DAPI) or 3.17% (act-caspase-3$^+$) Venus$^+$ cells were apoptotic, with small variations across regions. Other cells, mostly neurons, were also found to be activated caspase-3$^+$ (Fig. 1k), due to postnatal circuitry refinement. Given that the average time for an apoptotic cell to be removed from the brain is about 80 minutes (Sierra et al., 2013), and assuming that the clearance rates remain constant until adulthood, we estimated that the infiltrated monocytes could be removed from the brain parenchyma within approximately 42-72h. Although this is an estimation based

on the mean rate of observed apoptosis, it helps explain the drop in Venus^{+} cell numbers detected from P3 to P6 (Fig. 1e).

In light of these data, we conclude that the adult microglial population is composed exclusively from yolk sac derived cells, without the contribution of hematopoietic derived monocytes infiltrating at perinatal stages.

The number of microglial cells remains stable throughout life in mice and humans

We next investigated the regional and temporal changes in the number of microglial cells in a select number of brain regions, in order to understand their population dynamics. The density of murine microglial cells (Iba1^{+}) remained remarkably stable throughout, with little change from the young (4-6 months) to the aged (18-24 months) brains in all the areas analysed, except in the thalamus, where an increased number was found with ageing (Fig. 2a). Microglial cells were more dense in grey matter enriched vs. white matter enriched areas, as previously shown (Lawson et al., 1990). To better understand if the maintenance of microglial numbers was achieved by local self-renewal or by a contribution from circulating monocytes, we compared the microglial density in young vs. aged CCR2$^{-/-}$ and WT mice. CCR2$^{-/-}$ monocytes have deficient egress from the bone marrow, leading to fewer circulating monocytes (Serbina and Pamer, 2006), making them a valuable model in which to study the role of recruited monocytes (Gomez-Nicola and Perry, 2015). The contribution of patrolling monocytes (CX3CR1^{+}/CCR2^{-}) was not studied by our approach and cannot be excluded, although these cells have been shown to infiltrate the CNS only under pathological conditions (Shechter et al., 2013). Neither young, nor aged, CCR2$^{-/-}$ mice had a different number of microglial cells when compared to WT mice (Fig. 2b),

suggesting that circulating monocytes do not contribute significantly to the microglial population during a healthy lifetime.

A similar picture was observed when we compared young (20-35 years old) vs. aged (58-76 years old) human cases. The density of microglia in the grey or white matter of the temporal cortex was found to be unchanged with ageing (Fig. 2c). Microglial cell density was greater in the white matter than grey matter (Fig. 2c, 2d), in agreement with previous findings (Mittelbronn et al., 2001). This pattern of distribution is opposed to that previously found in rodents (Lawson et al., 1990), indicating species-specific regional differences in the microglial population.

Together, these data demonstrate that the density of microglial cells is remarkably stable in young and aged brains from both mice and humans.

The analysis of microglia in aged mice led to the identification of small numbers of multinucleated microglial aggregates (Fig. 2e), previously described in the aged rat brain (Perry et al., 1993). Multinucleated microglial aggregates were more frequent in the aged thalamus and cerebellum (Fig. S1a), and expressed MHCII (Fig. S1b) as well as CD45 (not shown). Using confocal microscopy we could identify aggregates containing up to 10 nuclei within the same cytoplasmic syncytium (Fig. S1c). To better understand if failed cytokinesis after increased proliferation was the origin of these aggregates we performed analysis of proliferation after repeated BrdU incorporation, by confocal microscopy (Fig. S1d). The incorporation of BrdU was minimal in these aggregates (0.48% were $BrdU^+$ and showed only 2 cells/aggregate; Fig. S1d), ruling out the hypothesis of failed cytokinesis. Our next hypothesis was that these aggregates could have a peripheral origin, which was confirmed after observing that aged $CCR2^{-/-}$ mice were devoid of multinucleated microglial aggregates (Fig. 2f).

Microglia have a high proliferation rate in the mouse and human brain

Although it is often assumed that the microglial population is maintained by a slow turnover of long-lived resident cells, little formal evidence exists (reviewed in (Gomez-Nicola and Perry, 2015)). Earlier work from Lawson and colleagues (Lawson et al., 1992), using H^3 thymidine combined with immunohistochemistry for F4/80, demonstrated that microglia proliferate in the healthy brain, but more slowly than other tissue macrophages: 0.05% of the microglia were proliferating at a given time, 20-times less than the lowest labelling index for any other resident macrophage populations studied (Lawson et al., 1992). We set out to analyse the proliferation of resident microglia by using more sensitive techniques (BrdU incorporation detected in $Iba1^+$ cells by double immunohistochemistry of DAB and AP)(Olmos-Alonso et al., 2016). We found that microglial proliferation rates in the adult brain were approximately 10-times higher (Fig. 3a, 3b, 3c) than those previously reported by Lawson et al., 1992. On average, 0.69% of the total microglial cells were proliferating ($Iba1^+$ $BrdU^+$) after a single pulse of BrdU. This rate was particularly high in the dentate gyrus (DG), the only area where we also found that ageing had an impact on the proliferation rate (Fig. 3a, 3b, 3c). We ensured that these rates were not underestimated by the dose of BrdU, since we had performed a dose-response analysis of microglial proliferation confirming that the BrdU dose (7.5mg/ml) used was optimal (Fig. S2a, S2b). We next performed a time-course analysis of proliferation/division after a single pulse of BrdU in microglial cells (Fig. 3b). In the cortex we could detect the duplication of the proliferating population from 16h after the BrdU pulse, indicating successful cell cycle exit and cell division (Fig. 3b). Return to the baseline number of $Iba1^+BrdU^+$ cells was observed from 24h. Considering that the S phase of mammalian cells comprises ~50% of the duration of the cell cycle, with G_2/M only taking a few hours (Cameron and Greulich, 1963), this allows an

estimate of a cell cycle length (*Tc*) of 32h. This would be in agreement with reported cell cycle lengths of macrophages, which vary depending on differentiation stage from 20-40h (Kueh et al., 2013). If S phase spans ~50% of the cell cycle length our data from BrdU labelling would only detect half of the dividing population. This indicates that ~1.38% of the population will be proliferating at a given time (*F*=fraction of cells in cell cycle). If we use these rates to calculate the time needed for the entire rodent microglial population to renew (*X*), with the equation:

$$X = \frac{100xTc}{F}$$

we can estimate the population renews once every 2318 hours (~96 days), allowing as many as 6 cycles of complete renewal during an animal's lifetime (average 21 months). However, these calculations are based on estimations of *Tc*, and require further specific study in the future.

The proliferative cycle was much quicker in the DG, where the initial duplication returned to baseline before 24h (Fig. 3b). In addition to revealing the higher proliferative activity of microglia in the DG, these data strongly suggest that microglial death must be tightly temporally and spatially coupled to proliferation, in order to maintain the stable density of microglial cells, as discussed below.

Higher figures were observed when analysing the proliferation of human microglia (on average, 2% of the microglial population proliferating at a given time), according to double staining of Iba1 and Ki67 (Fig. 3d, 3e). This rate is 2.9x higher than that observed for mice above (0.69%). However, Ki67 expression is not directly comparable to BrdU incorporation. This difference might be explained by the fact that Ki67 would label not only the S-phase but also other cell cycle phases except G0. This means that the labelling of Ki67 is approximately 2x higher than BrdU (Kee et al., 2002), which only labels S phase comprising ~50% of the duration of the cell

cycle (Cameron and Greulich, 1963). If cell cycle length remains constant in mammals (32h, above), this would allow an estimation of hundreds of cycles of complete renewal during lifetime (average 80 years).

To further explore any age-related changes in microglial proliferation, we studied the expression of genes related to the CSF1R driven proliferative response (Gomez-Nicola et al., 2013). We found a significant reduction in the expression of *PU.1* and *IRF8* in ageing brains, and a non-significant trend towards a reduction in relevant genes like *CSF1, CSF1R, C/EBPα, CD34* or *RUNX1* (Fig. S3). To further address the significance of the CSF1R pathway in controlling microglial turnover, we administered young mice with a diet containing GW2580, a specific CSF1R inhibitor previously shown to cause blockade of microglial proliferation but not their survival (Gomez-Nicola et al., 2013, Uitdehaag et al., 2011, De Lucia et al., 2016, Olmos-Alonso et al., 2016), in contrast to the microglia-depleting effects caused by the CSF1R inhibitor PLX3397 (Elmore et al., 2014). Treatment with GW2580 for 3 months decreased the total number of microglial cells ($PU.1^+$) by 17% (Fig. 3f, 3g), supporting the relevance of the CSF1R pathway in controlling the homeostatic maintenance of microglial turnover.

To provide an independent method to validate our analysis of microglial proliferation in mice, we took advantage of the ability of γ-retroviral vectors to selectively transduce proliferating glial cells (Gomez-Nicola et al., 2014). We delivered an Eco-SFFV γ-retroviral vector driving the expression of mCherry to the lateral ventricle of c-fms EGFP mice, allowing diffusion to adjacent areas (cortex and striatum) due to the initially injected volume (5μl)(Fig. 3h). We analysed the incorporation of Eco-SFFV-RV mCherry 3 days after injection, to allow for the expression of detectable levels of mCherry (Gomez-Nicola et al., 2014) and to allow the potential visualization of pairs

of cells, before post-division microglial death (Fig. 3b). We found a limited number of microglial cells ($EGFP^+$) expressing mCherry, presenting as typical microglial duplets (Fig. 3i). The quantification of proliferating microglial cells ($mCherry^+EGFP^+$) offered a similar proliferation rate (Fig. 3j) as that previously described by analysing the incorporation of BrdU in Iba1 cells (Fig. 3a), validating our previous findings.

For direct visualisation of microglial turnover, we used chronic live imaging of the olfactory bulb microglia in $CX_3CR1^{GFP/+}$ mice, coupled to repeated blood vessel imaging (Kovalchuk et al., 2015)(Fig. S4a). To control for potential interference of the implantation of the chronic window on the microglial behaviour, mice were analysed 3-4 weeks after surgery, to allow initial inflammation to resolve. After this, imaged microglia were typical highly branched, $CD11b^{low}$ and $CD68^-$ (Fig. S4b, S4c), and therefore considered as surveillant microglia. Repeated live imaging of microglia allowed the identification of cell division (duplication; Fig. 3k) or death (disappearance; Fig. 6a), and defined the proliferation rate of microglia at 0.79% per day (Fig. 3l), similar to the rate we found with Iba1/BrdU staining (Fig 3a). During the first 24h after division, paired microglia were found at a significantly closer distance than resident non-dividing microglia (Fig. 3m), suggesting that these cells were generated from the same proliferating cell. During the following days the cells migrated away from each other and reached cell-to-cell dispersion similar to the rest of the microglial population within 3-4 days (Fig. 3n). These data confirm the high rates of microglial proliferation detected by Iba1/BrdU staining and suggest that the territories occupied by microglia change upon cell division, probably affecting the performance of local homeostatic functions.

Thus, using three independent lines of evidence our data show that microglia proliferate in the adult mouse and human brain at a high rate, allowing several cycles of renewal of the whole population during the organism's lifetime.

Microglial turnover is not maintained by Nestin^{+} precursors

In light of recent findings suggesting that Nestin^{+} microglial precursors may be involved in the repopulation response after pharmacological (Elmore et al., 2014) or transgenic microglial ablation (Bruttger et al., 2015), we aimed to study if microglial proliferation in the steady-state was maintained by a subpopulation of stem cell-like microglia. We analysed Nestin-GFP mice, as an optimal reporter mouse for the expression of nestin (Mignone et al., 2004), and although we evidenced the previously reported expression in pericytes (Figure 4a, 4b, 4c), neural stem cells (Figure 4b) and oligodendrocyte precursor cells (Figure 4a, 4c)(Mignone et al., 2004), we did not find any evidence of nestin expression in microglia (Iba1^{+}; Figure 4a, 4b, 4c). We specifically studied the expression of nestin in proliferating microglia (Iba1^{+}BrdU^{+}; 24h post-injection), and found no evidence of nestin^{+} microglia (Figure 4d). We therefore conclude that microglial proliferation is not maintained by Nestin^{+} microglial precursors in the steady state.

Microglial proliferation and apoptosis are temporally and spatially coupled to maintain microglial homeostasis

The time-course analysis of microglial proliferation (Fig. 3b) suggested that microglial cell death plays a key role in maintaining the stable number of microglia over time. Given the difficulties of analysing microglial apoptosis by traditional methods (Sierra et al., 2013) we set out to address this point by using live imaging of microglia in $CX_3CR1^{GFP/+}$ mice. Under these conditions, microglial death is defined as a disappearance of a cell within the network of relatively immobile neighbouring cells (Fig. 5a) with the blood vessel pattern serving as additional landmarks. The death rate of resident microglia was found to be 1.23% per day, while the death rate for

newborn (recently divided) microglia was 2.40% (Fig. 5b). For newborn microglial cells the death rate was highest during the first 5 days after division (5.0 ± 3.5%), significantly higher than the death rate in the resident adult cell population.

To further study the relevance of microglial apoptosis in the maintenance of the population we studied the numbers of microglia in three mouse models defective in intrinsic apoptosis (PUMA$^{-/-}$, BIM$^{-/-}$ and Vav-Bcl2). While the first two have ubiquitous deletion of the pro-apoptotic BH3-only molecules PUMA or BIM, the Vav-Bcl2 mice have the anti-apoptotic molecule Bcl2 overexpressed only in cells of the myeloid lineage. When compared to WT mice, both BIM$^{-/-}$ and Vav-Bcl2 mice were found to have a significant increase in the number of microglial cells (Fig. 5c). PUMA$^{-/-}$ showed no difference, or even a reduction, in the number of microglia (Fig. 5c), in agreement with previous findings in the eye (Zhang et al., 2012) and suggesting that microglial apoptosis is PUMA-independent. Since Vav-Bcl2 mice provide a robust block in intrinsic apoptosis only in lymphoid and myeloid lineage cells (Egle et al., 2004), which in the brain is restricted to microglia, we decided to focus on the study of this model (Fig. 5d). A time-course of postnatal development of the microglial population in Vav-Bcl2 mice showed that the increase in number of microglial cells is reached early in life (P44) and remains stable until middle-age (before the onset of other health defects (Egle et al., 2004))(Fig. 5e, 5f). This stabilization of increased density, caused by deficient microglial apoptosis, is perhaps explained by the inability of the parenchyma to accommodate more cells, suggesting contact inhibition mechanisms are in place.

In order to understand the impact of apoptosis blockade on microglial phenotype, we isolated microglia by FACS and analysed their transcriptomic profile by RNAseq (Fig. 6). Flow cytometry analysis showed a significant increase in the population of CD11b^{+}CD45^{high} cells in Vav Bcl-2 mice, when compared to WT littermates (Fig. 6a),

identifying this subpopulation of microglia as the biggest contributor to increased numbers observed previously. Isolation of $CD11b^{+}CD45^{low}$ and $CD11b^{+}CD45^{high}$ subpopulations from WT and Vav Bcl-2 followed by RNAseq profiling rendered a total of 137 genes statistically (P <0.01; fold change >10) upregulated in Vav Bcl-2 vs WT and 259 statistically downregulated in Vav Bcl-2 vs WT microglia (Fig. 6b; Table S1). Gene Ontology analysis revealed differentially expressed genes were particularly associated with GO-Slim terms involved in metabolic processes and biogenesis (Fig. 6c). Clustering of GO terms (based on genes shared between each GO category) revealed GO processes previously identified to be upregulated in microglia (Grabert et al., 2016), including immune response and macromolecule biosynthesis (Fig. 6d), amongst others. Vav Bcl-2 mice also showed a significant alteration of genes clustered under the processes of cell cycle and proliferation and death, confirming the expected effects of Bcl-2 upregulation (Fig. 6c). Vav Bcl-2 microglia had a significant repression (> 200-fold) of the pro-apoptotic gene Bad, and a significant upregulation (17-fold) of the anti-apoptotic gene Api5 (Table S1). Also Vav Bcl-2 microglia showed a significant repression of cell cycle promoting genes like Mad2l1, Mdm2, Cdca3, Cdk1, Cdc20 and Cdc20b (all > 25-fold down-regulated) (Table S1). These changes confirm the anti-apoptotic effects of Bcl-2 overexpression in microglia, but also suggest an impaired cell cycle regulation as an associated effect. A Venn diagram showing the relations between the gene sets of $CD45^{low}$ and $CD45^{high}$ identifies the $CD11b^{+}CD45^{low}$ subpopulation as the major contributor to the transcriptional variability observed between WT and Vav Bcl-2 microglia (Fig. 6e).

Despite the fact that Vav-Bcl2 mice had a significant alteration in the number and phenotype of microglia through most of their adult life, they did not display gross deficiencies in the astrocyte (Fig. S5a) or the neuronal (Fig. S5b) populations, and only showed minor differences in age-dependent changes in synaptic density (Fig.

S5c). Vav-Bcl2 mice showed no differences in behavioural performance when compared to WT mice (Fig. S6a, S6b).

We next analysed the temporal and spatial relationship between death and proliferation events in vivo. We observed a remarkably rapid reorganisation of the microglial landscape (Fig. 7a). This is exemplified by the representation of the history of microglia during the 22-day-long imaging period in a sample field of view, with stable cells shown in grey, cells going to die shown in red and cells going to divide shown in blue (Fig. 7b). Microglial proliferation and apoptosis were spatially and temporally coupled, as many more cells proliferated in the vicinity (≤ 200 μm) of a dying cell immediately after its death (Fig. 7c). Some of the proliferating cells were immediately adjacent to the dying cells, whereas others were located more distantly (Fig. 7b, 7d). The median distance between the dying and the nearest proliferating cell was 72.95±43.13 μm (n=19 cell pairs), being almost double the distance between the dying and the nearest resident cell (37.94±11.74 μm, n=31 cell pair) (Fig. 7d, 7e). Thus overall, proliferating cells were found to be the second closest neighbour to the dying cells.

In summary, our data indicate that the microglial population undergoes a constant and rapid remodelling, based on the temporal and spatial coupling of proliferation and apoptosis, providing a mechanism for the homeostasis of the population through life. This constant renewal causes not only the individual cellular players to change, but also their spatial layout to be rapidly modified.

DISCUSSION

During the last decade, the study of microglial cells and neuroinflammation has experienced a revolution. Minimally-invasive methods have revealed microglia to be highly dynamic in their interaction with the microenvironment, responding to inflammatory signals (Nimmerjahn et al., 2005, Davalos et al., 2005) and interacting with neuronal circuits at the synaptic level (Tremblay et al., 2010, Wake et al., 2009). Microglia can sculpt the brain and impact on its physiology, as they have been observed to contain phagocytic inclusions with features of axonal terminals, dendritic spines or unneeded neuronal progenitors (Tremblay et al., 2010, Paolicelli et al., 2011, Sierra et al., 2010). Our data demonstrate that microglial cells are actively renewed and that the brain population is maintained by a finely tuned balance of proliferation and apoptosis.

It has been long assumed that microglia are “long-lived” cells. At the population level, microglia are indeed long-lived, but at the individual cell level they are not. The microglial landscape changes radically within a few weeks, with cells dying, other taking their place and their absolute position changing. This renewing landscape will likely influence the interpretation of phenomena such as microglial priming, where the microglial response is exaggerated (stronger than that observed in stimulus-naive microglia) to a secondary insult. This is perhaps best illustrated when the first (priming) and second stimulus are separated by prolonged periods of time, in the context of adult responses to early-life infections (Bilbo and Schwarz, 2009), delayed inflammation after TBI (Johnson et al., 2013) or the onset of age-related amyloid deposition after gestational inflammation (Krstic et al., 2012). There, microglial priming implies the need for “microglial memory” to the first stimulus to elicit an exaggerated response to the second stimulus. We suggest that our findings could

either support the hypothesis that microglial priming is achieved through epigenetic (inheritable) changes (Schwarz et al., 2011) or suggest that “microglia memory” could be stored elsewhere in the neural/glial network. We believe that the parameters defined here will stimulate a re-interpretation of many of the functions of microglia in health and disease.

The fact that the adult microglial population is maintained at least in part by self-renewal has been largely assumed for over 2 decades, since our group reported on the proliferation of resident microglia (Lawson et al., 1992). Using [3H]-thymidine incorporation and detection with autoradiography, Lawson *et al*, described a very low turnover rate for microglia, with ~0.05% of the cells dividing at a time (Lawson et al., 1992). Although a probable underestimation, acknowledged at the time due to the relative insensitivity of the method, these studies were never revisited using the gold standard in the field: incorporation of BrdU. We now show, using three independent methods, that the proliferation index of microglia is much higher than expected (more than 10x higher), and an average of 0.69% microglial cells are in S phase at a given time. This rate would allow for an estimation of the brain’s microglial population being renewed every ~95 days, allowing several cycles of renewal within the lifetime of a mouse. Higher rates are found in the human brain (average 2%), with a more dramatic consequence on the turnover cycles: leading to estimates that microglia would cycle hundreds of times during 80 years of life. However, the estimation of the turnover rate of human microglia would need alternative methods in order to provide a more accurate calculation and allow extrapolation to the average human population.

This homeostatic microglial proliferation is balanced by the opposing force of microglial apoptosis. The apoptotic cascade controlling microglial death seems to be

dependent on the pro-apoptotic molecule BIM but not PUMA, as evidenced from the analysis of KO mice. A recent report demonstrated that deficiency in PUMA leads to decreased numbers of both retinal and brain microglia, due to unexpected roles of this protein in promoting cell survival (Zhang et al., 2012), consistent with our present findings showing a decreased density of microglia in PUMA$^{-/-}$ mice. Microglial death can be counteracted by the inhibition of mitochondrial apoptosis as indicated by the overexpression of Bcl2 leading to increased microglial numbers. Surprisingly, our results support the hypothesis that the brain can only accommodate certain number of microglial cells, as deficient microglial death causes the increased microglial numbers to plateau after postnatal development. In the normal brain, the microglial population displays a mosaic-like organization where processes of individual cells avoid contact with each other, being disrupted only with the emergence of changes related to pathology, age or systemic influences (Gomez-Nicola and Perry, 2015). Transcriptomic profiling of microglia from Vav Bcl-2 mice highlights profound alterations of their functional profile, including altered metabolism and immune response, providing a link between homeostatic microglial apoptosis with phenotypic profile. A more detailed future study of the mechanisms by which altered microglia turnover could impact basic microglia functions, including those controlling their inflammatory properties, will provide valuable insights to understand the maintenance of the microglial population in health and disease.

The sub-regional analysis of microglial turnover highlighted the DG as a particularly active anatomical region. In the DG, microglial proliferation is higher, quicker and decays more rapidly with age. An age-dependent decrease in proliferation is also observed in the population of DG neural progenitors (Kuhn et al., 1996), and this can be correlated with the decrease of microglial proliferation, as microglial phagocytosis

of progenitors is coupled to neurogenic activity (Sierra et al., 2010). Thus, ageing would lead to a decrease in DG microglial proliferation indirectly, through a decline in neurogenesis. A more direct effect of ageing on microglia residing within the DG would imply microglial senescence. Replicative senescence, the loss of mitotic potential accompanied by significant telomere shortening, occurs once a cell has undergone approximately 50 replications, the so-called Hayflick limit (Hayflick, 1965). Thus, we hypothesise that the increased microglial turnover in the DG will lead to a quicker extinction of the proliferative capacity of these cells, as observed in our data. The microglial population at the DG seems particularly susceptible to telomere shortening, as recently highlighted using a mouse model of telomere dysfunction (TERC KO)(Khan et al., 2015), supporting the hypothesis that increased microglial division can lead to replicative senescence.

In an attempt to reconcile conflicting evidence about the contribution of circulating monocytes to the composition of the microglial population at perinatal stages (Ginhoux et al., 2013), we developed a cell-tracking approach based on the intra-liver tracing of embryonic haematopoiesis. Our results support the existence of a wave of monocytes that infiltrate the brain, peaking at P3, but indicate that these are rapidly depleted by apoptosis and do not contribute to the final microglial population, which we can now confirm is exclusively formed by yolk-sac derived progenitors. The elimination of infiltrated macrophages is coincident with a wave of microglial proliferation, followed by a further selection process before the final number of cells is achieved (Nikodemova et al., 2015). The functional significance of this wave of liver-derived monocytes is unknown, and should be the subject of future research, but the temporal coincidence with the refinement of the microglial numbers prompts

speculation that these cells could trigger the death of a subpopulation of yolk sac derived microglia.

The changes in microglial morphology that occur during ageing are well documented, however, a particular morphological change that has received little attention to date is the formation of giant, multinucleated microglial aggregates in aged mice, such as those observed in our study. Previous studies have shown that microglia form aggregates with multiple nuclei, which can include more than 20 individual cells, under certain inflammatory conditions (Fendrick et al., 2007, Perry et al., 1993). Our data show that these aggregates are not generated by failed cytokinesis after division. Similar structures are observed in the context of a repopulation paradigm after genetic ablation of microglia (Bruttger et al., 2015). However, these clusters are $BrdU^+$ (Bruttger et al., 2015), transient and not fused, suggesting they serve as pools of repopulating microglia, whereas we here observe a fusion/aggregation of groups of cells. Given the territorial nature and lack of contact between microglial cells in younger brains, this is seen as an aberrant morphological development and represents a significant change in the phenotype and function of microglia in ageing. With our data we can provide clear evidence that these aggregates likely originate from the incorporation of circulating monocytes into the brain parenchyma, but further research is needed to fully understand their function.

One question of particular interest raised by our data is the molecular regulation of the self-renewal process. We provide evidence for a necessary, but not sufficient, role of CSF1R in controlling microglial turnover in homeostasis, as is evidenced from our mRNA studies and from the pharmacological inhibition of the CSF1R tyrosine kinase activity with GW2580. Elimination of microglia can be achieved by acute

treatment with a highly potent CSF1R/c-kit/FLT3/PDGFRβ inhibitor, highlighting the relevance of these receptors in maintaining microglial numbers (Elmore et al., 2014). However, other systems may have to be in place to fully control microglial turnover. Recent studies, using genetic ablation of microglia, show that IL-1R plays a crucial role in the replenishment process (Bruttger et al., 2015). Although a repopulation process cannot be compared to the homeostatic maintenance of the microglial population, complementary systems (CSF1R, IL1R, or others) must be in place in order to ensure the stability of this important population of non-neuronal cells in the CNS.

In light of the current data, we conclude that the turnover of the microglial population is a highly dynamic process, made possible due to the finely tuned temporal and spatial balance of microglial proliferation and apoptosis. Our data question the view of microglia as a long-lived population, almost never renewed in the adult brain, and propose a much more dynamic scenario, which will help uncover the key microglial functions in the healthy and diseased brain.

EXPERIMENTAL PROCEDURES

Experimental mice

All experimental procedures were either approved by a local ethical review committee and conducted in accordance with personal and project licenses under the UK Animals (Scientific Procedures) Act (1986), or performed in accordance with institutional animal welfare guidelines and were approved by the government of Baden-Wurttemberg, Germany. Details of experimental mice can be found in the Supplementary information.

To analyse cell proliferation, mice received injections of i.p. BrdU (Sigma-Aldrich; 7.5mg/ml, 0.1ml/10g weight in sterile saline). A dose-response experiment was performed using 3.75, 7.5 or 15mg/ml BrdU.

Post-mortem human brain samples

For immunohistochemical analysis, human brain autopsy tissue samples (n=15 per group)(temporal cortex, paraffin-embedded, formalin-fixed, 96% formic acid-treated, 6μm sections) from the National CJD Surveillance Unit Brain Bank (Edinburgh, UK) were obtained from Alzheimer's disease or vCJD non-diseased age- and sex-matched young (age 20-35) or aged (age 58-79) controls, in whom consent for use of autopsy tissues for research had been obtained. Ethical permission for research on autopsy materials stored in the National CJD Surveillance Unit was obtained from Lothian Region Ethics Committee.

In utero intra-liver tracing of embryonic haematopoiesis

Cell tracking was performed by the administration of VSVG-SFFV-Venus or VSVG-SFFV-mCherry lentiviral vectors. Details on the design, production and application of these vectors can be found in the Supplementary information.

Chronic cranial window implantation

Chronic cranial window was installed as previously described(Kovalchuk et al., 2015). A detailed description of the method can be found in the Supplementary information.

Two-photon Imaging

Microglia expressing eGFP in the OB of $CX_3CR1^{GFP/+}$ mice were imaged once a day for 10 to 22 days by means of two-photon microscopy. Details of the method can be found in the supplementary information.

Immunohistochemistry

Coronal hippocampal sections were cut from paraformaldehyde-fixed, frozen or fresh brains. Mice perfusion, tissue processing and immunohistochemical analysis was performed as previously described(Gomez-Nicola et al., 2013), with details found in the supplementary information.

Statistical Analysis

Data were expressed as mean±SEM and analysed with the GraphPad Prism 5 software package (GraphPad Software). When normality and homoscedasticity assumptions were reached, we applied the two-tailed Fisher T-test, the one-way or two-way ANOVA, followed by the Tukey post-hoc test for multiple comparisons. For the analysis of two-photon imaging, for normally distributed data, mean±SEM was calculated and the Student's t test was used for comparison of two groups. For data that were not normally distributed, the median±one interquartile range was presented as box plot, and 10 to 90 percentiles were shown as whiskers. For comparisons between non-parametrically distributed groups we used Mann-Whitney test. Wilcoxon

matched pairs test was used for nonparametric comparison of two paired groups. All the statistical tests were two sided. Differences were considered significant for $p<0.05$.

Author contributions

D.G-N., V.H.P. and O.G. conceived and designed the study. K.A., Y.L., A.O-A, F.G-M., K.L., P.R., T.T., M.A.C. and D.G-N. performed the in vivo experimental work and analysed the experimental data. K.R., Z.M., A.S., S.B., M.S.C., O.G. and V.H.P. provided reagents, equipment and/or experimental samples. D.G-N. supervised the study and wrote the manuscript. All authors edited and approved the manuscript. Competing interests: The authors have no conflicting financial interests.

Acknowledgements

We thank the National CJD Surveillance Unit Brain Bank (Edinburgh, UK) for the provision of human samples. We thank Prof. Andreas Strasser (Melbourne, Australia) for the gift of the Vav-Bcl-2 mice and Prof. Axel Schambach (MH Hannover, Germany) for the γ-retroviral vector RSF91.GFP.pre* and the packaging plasmid pcDNA3.MLVgp. The research was funded by the Medical Research Council (MR/K022687/1), by a Vice-Chancellor PhD studentship (K.A.), by grants from the Spanish Ministry of Economy and Competitiveness with FEDER funds (BFU2015-66689, RYC-2013-12817) and by the Alzheimer Forschung Initiative e.V.

References

ALLIOT, F., GODIN, I. & PESSAC, B. 1999. Microglia derive from progenitors, originating from the yolk sac, and which proliferate in the brain. *Brain Res Dev Brain Res,* 117**,** 145-52.

BILBO, S. D. & SCHWARZ, J. M. 2009. Early-life programming of later-life brain and behavior: a critical role for the immune system. *Front Behav Neurosci,* 3**,** 14.

BRUTTGER, J., KARRAM, K., WORTGE, S., REGEN, T., MARINI, F., HOPPMANN, N., KLEIN, M., BLANK, T., YONA, S., WOLF, Y., MACK, M., PINTEAUX, E., MULLER, W., ZIPP, F., BINDER, H., BOPP, T., PRINZ, M., JUNG, S. & WAISMAN, A. 2015. Genetic Cell Ablation Reveals Clusters of Local Self-Renewing Microglia in the Mammalian Central Nervous System. *Immunity,* 43**,** 92-106.

CAMERON, I. L. & GREULICH, R. C. 1963. Evidence for an essentially constant duration of DNA synthesis in renewing epithelia of the adult mouse. *J Cell Biol,* 18**,** 31-40.

CUNNINGHAM, C. L., MARTINEZ-CERDENO, V. & NOCTOR, S. C. 2013. Microglia regulate the number of neural precursor cells in the developing cerebral cortex. *J Neurosci,* 33**,** 4216-33.

DAVALOS, D., GRUTZENDLER, J., YANG, G., KIM, J. V., ZUO, Y., JUNG, S., LITTMAN, D. R., DUSTIN, M. L. & GAN, W. B. 2005. ATP mediates rapid microglial response to local brain injury in vivo. *Nat.Neurosci.,* 8**,** 752-758.

DE LUCIA, C., RINCHON, A., OLMOS-ALONSO, A., RIECKEN, K., FEHSE, B., BOCHE, D., PERRY, V. H. & GOMEZ-NICOLA, D. 2016. Microglia regulate hippocampal neurogenesis during chronic neurodegeneration. *Brain Behav Immun,* 55**,** 179-90.

EGLE, A., HARRIS, A. W., BATH, M. L., O'REILLY, L. & CORY, S. 2004. VavP-Bcl2 transgenic mice develop follicular lymphoma preceded by germinal center hyperplasia. *Blood,* 103**,** 2276-83.

ELMORE, M. R., NAJAFI, A. R., KOIKE, M. A., DAGHER, N. N., SPANGENBERG, E. E., RICE, R. A., KITAZAWA, M., MATUSOW, B., NGUYEN, H., WEST, B. L. & GREEN, K. N. 2014. Colony-stimulating factor 1 receptor signaling is necessary for microglia viability, unmasking a microglia progenitor cell in the adult brain. *Neuron,* 82**,** 380-97.

FENDRICK, S. E., XUE, Q. S. & STREIT, W. J. 2007. Formation of multinucleated giant cells and microglial degeneration in rats expressing a mutant Cu/Zn superoxide dismutase gene. *J Neuroinflammation,* 4**,** 9.

GINHOUX, F., GRETER, M., LEBOEUF, M., NANDI, S., SEE, P., GOKHAN, S., MEHLER, M. F., CONWAY, S. J., NG, L. G., STANLEY, E. R., SAMOKHVALOV, I. M. & MERAD, M. 2010. Fate mapping analysis reveals that adult microglia derive from primitive macrophages. *Science,* 330**,** 841-5.

GINHOUX, F., LIM, S., HOEFFEL, G., LOW, D. & HUBER, T. 2013. Origin and differentiation of microglia. *Front Cell Neurosci,* 7**,** 45.

GOMEZ-NICOLA, D., FRANSEN, N. L., SUZZI, S. & PERRY, V. H. 2013. Regulation of microglial proliferation during chronic neurodegeneration. *J Neurosci,* 33**,** 2481-93.

GOMEZ-NICOLA, D. & PERRY, V. H. 2015. Microglial dynamics and role in the healthy and diseased brain: a paradigm of functional plasticity. *Neuroscientist,* 21**,** 169-84.

GOMEZ-NICOLA, D., RIECKEN, K., FEHSE, B. & PERRY, V. H. 2014. In-vivo RGB marking and multicolour single-cell tracking in the adult brain. *Sci Rep,* 4**,** 7520.

GRABERT, K., MICHOEL, T., KARAVOLOS, M. H., CLOHISEY, S., BAILLIE, J. K., STEVENS, M. P., FREEMAN, T. C., SUMMERS, K. M. & MCCOLL, B. W. 2016. Microglial brain region-dependent diversity and selective regional sensitivities to aging. *Nat Neurosci,* 19**,** 504-16.

HASHIMOTO, D., CHOW, A., NOIZAT, C., TEO, P., BEASLEY, M. B., LEBOEUF, M., BECKER, C. D., SEE, P., PRICE, J., LUCAS, D., GRETER, M., MORTHA, A., BOYER, S. W., FORSBERG, E. C., TANAKA, M., VAN ROOIJEN, N., GARCIA-SASTRE, A., STANLEY, E. R., GINHOUX, F., FRENETTE, P. S. & MERAD, M. 2013. Tissue-resident macrophages self-maintain locally throughout adult life with minimal contribution from circulating monocytes. *Immunity,* 38**,** 792-804.

HAYFLICK, L. 1965. The Limited in Vitro Lifetime of Human Diploid Cell Strains. *Exp Cell Res,* 37**,** 614-36.

HOEFFEL, G., CHEN, J., LAVIN, Y., LOW, D., ALMEIDA, F. F., SEE, P., BEAUDIN, A. E., LUM, J., LOW, I., FORSBERG, E. C., POIDINGER, M., ZOLEZZI, F., LARBI, A., NG, L. G., CHAN, J. K., GRETER, M., BECHER, B., SAMOKHVALOV, I. M., MERAD, M. & GINHOUX, F. 2015. C-Myb(+) erythro-myeloid progenitor-derived fetal monocytes give rise to adult tissue-resident macrophages. *Immunity,* 42**,** 665-78.

JOHNSON, V. E., STEWART, J. E., BEGBIE, F. D., TROJANOWSKI, J. Q., SMITH, D. H. & STEWART, W. 2013. Inflammation and white matter degeneration persist for years after a single traumatic brain injury. *Brain,* 136**,** 28-42.

KEE, N., SIVALINGAM, S., BOONSTRA, R. & WOJTOWICZ, J. M. 2002. The utility of Ki-67 and BrdU as proliferative markers of adult neurogenesis. *J Neurosci Methods,* 115**,** 97-105.

KHAN, A. M., BABCOCK, A. A., SAEED, H., MYHRE, C. L., KASSEM, M. & FINSEN, B. 2015. Telomere dysfunction reduces microglial numbers without fully inducing an aging phenotype. *Neurobiol Aging,* 36**,** 2164-75.

KOVALCHUK, Y., HOMMA, R., LIANG, Y., MASLYUKOV, A., HERMES, M., THESTRUP, T., GRIESBECK, O., NINKOVIC, J., COHEN, L. B. & GARASCHUK, O. 2015. In vivo odourant response properties of migrating adult-born neurons in the mouse olfactory bulb. *Nat Commun,* 6**,** 6349.

KRSTIC, D., MADHUSUDAN, A., DOEHNER, J., VOGEL, P., NOTTER, T., IMHOF, C., MANALASTAS, A., HILFIKER, M., PFISTER, S., SCHWERDEL, C., RIETHER, C., MEYER, U. & KNUESEL, I. 2012. Systemic immune challenges trigger and drive Alzheimer-like neuropathology in mice. *J Neuroinflammation,* 9**,** 151.

KUEH, H. Y., CHAMPHEKAR, A., NUTT, S. L., ELOWITZ, M. B. & ROTHENBERG, E. V. 2013. Positive feedback between PU.1 and the cell cycle controls myeloid differentiation. *Science,* 341**,** 670-3.

KUHN, H. G., DICKINSON-ANSON, H. & GAGE, F. H. 1996. Neurogenesis in the dentate gyrus of the adult rat: age-related decrease of neuronal progenitor proliferation. *J Neurosci,* 16**,** 2027-33.

LAWSON, L. J., PERRY, V. H., DRI, P. & GORDON, S. 1990. Heterogeneity in the distribution and morphology of microglia in the normal adult mouse brain. *Neuroscience,* 39**,** 151-70.

LAWSON, L. J., PERRY, V. H. & GORDON, S. 1992. Turnover of resident microglia in the normal adult mouse brain. *Neuroscience,* 48**,** 405-15.

MIGNONE, J. L., KUKEKOV, V., CHIANG, A. S., STEINDLER, D. & ENIKOLOPOV, G. 2004. Neural stem and progenitor cells in nestin-GFP transgenic mice. *J Comp Neurol,* 469**,** 311-24.

MITTELBRONN, M., DIETZ, K., SCHLUESENER, H. J. & MEYERMANN, R. 2001. Local distribution of microglia in the normal adult human central nervous system differs by up to one order of magnitude. *Acta Neuropathol,* 101**,** 249-55.

NIKODEMOVA, M., KIMYON, R. S., DE, I., SMALL, A. L., COLLIER, L. S. & WATTERS, J. J. 2015. Microglial numbers attain adult levels after undergoing a rapid decrease in cell number in the third postnatal week. *J Neuroimmunol,* 278**,** 280-8.

NIMMERJAHN, A., KIRCHHOFF, F. & HELMCHEN, F. 2005. Resting microglial cells are highly dynamic surveillants of brain parenchyma in vivo. *Science,* 308**,** 1314-1318.

OLMOS-ALONSO, A., SCHETTERS, S. T., SRI, S., ASKEW, K., MANCUSO, R., VARGAS-CABALLERO, M., HOLSCHER, C., PERRY, V. H. & GOMEZ-NICOLA, D. 2016. Pharmacological targeting of CSF1R inhibits microglial proliferation and prevents the progression of Alzheimer's-like pathology. *Brain,* 139**,** 891-907.

PAOLICELLI, R. C., BOLASCO, G., PAGANI, F., MAGGI, L., SCIANNI, M., PANZANELLI, P., GIUSTETTO, M., FERREIRA, T. A., GUIDUCCI, E., DUMAS, L., RAGOZZINO, D. & GROSS, C. T. 2011. Synaptic pruning by microglia is necessary for normal brain development. *Science,* 333**,** 1456-8.

PERRY, V. H., MATYSZAK, M. K. & FEARN, S. 1993. Altered antigen expression of microglia in the aged rodent CNS. *Glia,* 7**,** 60-7.

SCHWARZ, J. M., HUTCHINSON, M. R. & BILBO, S. D. 2011. Early-life experience decreases drug-induced reinstatement of morphine CPP in adulthood via microglial-specific epigenetic programming of anti-inflammatory IL-10 expression. *J Neurosci,* 31**,** 17835-47.

SERBINA, N. V. & PAMER, E. G. 2006. Monocyte emigration from bone marrow during bacterial infection requires signals mediated by chemokine receptor CCR2. *Nat Immunol,* 7**,** 311-7.

SHECHTER, R., MILLER, O., YOVEL, G., ROSENZWEIG, N., LONDON, A., RUCKH, J., KIM, K. W., KLEIN, E., KALCHENKO, V., BENDEL, P., LIRA, S. A., JUNG, S. & SCHWARTZ, M. 2013. Recruitment of beneficial M2 macrophages to injured spinal cord is orchestrated by remote brain choroid plexus. *Immunity,* 38**,** 555-69.

SHENG, J., RUEDL, C. & KARJALAINEN, K. 2015. Most Tissue-Resident Macrophages Except Microglia Are Derived from Fetal Hematopoietic Stem Cells. *Immunity,* 43**,** 382-93.

SIERRA, A., ABIEGA, O., SHAHRAZ, A. & NEUMANN, H. 2013. Janus-faced microglia: beneficial and detrimental consequences of microglial phagocytosis. *Front Cell Neurosci,* 7**,** 6.

SIERRA, A., ENCINAS, J. M., DEUDERO, J. J., CHANCEY, J. H., ENIKOLOPOV, G., OVERSTREET-WADICHE, L. S., TSIRKA, S. E. & MALETIC-SAVATIC, M. 2010. Microglia shape adult hippocampal neurogenesis through apoptosis-coupled phagocytosis. *Cell Stem Cell,* 7**,** 483-95.

SQUARZONI, P., OLLER, G., HOEFFEL, G., PONT-LEZICA, L., ROSTAING, P., LOW, D., BESSIS, A., GINHOUX, F. & GAREL, S. 2014. Microglia modulate wiring of the embryonic forebrain. *Cell Rep,* 8**,** 1271-9.

TAMBUYZER, B. R., PONSAERTS, P. & NOUWEN, E. J. 2009. Microglia: gatekeepers of central nervous system immunology. *J Leukoc Biol,* 85**,** 352-70.

TREMBLAY, M. E., LOWERY, R. L. & MAJEWSKA, A. K. 2010. Microglial interactions with synapses are modulated by visual experience. *PLoS Biol,* 8**,** e1000527.

UITDEHAAG, J. C., SUNNEN, C. M., VAN DOORNMALEN, A. M., DE ROUW, N., OUBRIE, A., AZEVEDO, R., ZIEBELL, M., NICKBARG, E., KARSTENS, W. J. & RUYGROK, S. 2011. Multidimensional profiling of CSF1R screening hits and inhibitors: assessing cellular activity, target residence time, and selectivity in a higher throughput way. *J Biomol Screen,* 16**,** 1007-17.

VARVEL, N. H., GRATHWOHL, S. A., BAUMANN, F., LIEBIG, C., BOSCH, A., BRAWEK, B., THAL, D. R., CHARO, I. F., HEPPNER, F. L., AGUZZI, A., GARASCHUK, O., RANSOHOFF, R. M. & JUCKER, M. 2012. Microglial repopulation model reveals a robust homeostatic process for replacing CNS myeloid cells. *Proc Natl Acad Sci U S A,* 109**,** 18150-5.

WAKE, H., MOORHOUSE, A. J., JINNO, S., KOHSAKA, S. & NABEKURA, J. 2009. Resting microglia directly monitor the functional state of synapses in vivo and determine the fate of ischemic terminals. *J Neurosci,* 29**,** 3974-80.

ZHANG, F., LI, Y., TANG, Z., KUMAR, A., LEE, C., ZHANG, L., ZHU, C., KLOTZSCHE-VON AMELN, A., WANG, B., GAO, Z., ZHANG, S., LANGER, H. F., HOU, X., JENSEN, L., MA, W., WONG, W., CHAVAKIS, T., LIU, Y., CAO, Y. & LI, X. 2012. Proliferative and survival effects of PUMA promote angiogenesis. *Cell Rep,* 2**,** 1272-85.

Figure legends

Figure 1. A wave of infiltrating monocytes invades the brain at early postnatal stages, to be rapidly depleted and not contributing to the adult microglial population.

(a) Experimental design, illustrating the tracing of late embryonic haematopoiesis by the intra-utero marking of liver progenitors with VSVG-SFFV lentiviral vectors (E14) and subsequent analysis of brain infiltration (P0-P43). **(b, c)** Representative examples of Venus$^+$ (green) infiltrating cells at p3 (cerebellum), with migratory (bipolar, elongated) **(b)** or ramified (multiple radially orientated processes) **(b (right), c)** morphologies. Iba1 expression is shown in red in differentiated ramified cells. **(d, e)** Time-course analysis of the number of resident microglia (Iba1$^+$Venus$^-$) and infiltrating monocytes (Venus$^+$) in the postnatal cerebellum (CB), cortex (CX) and hippocampus (HC). Note that at all ages tested Venus$^+$ cells **(e)** represent only a minority of all Iba$^+$ cells **(d)**. **(g, h)** Phenotypic characterization of Venus$^+$ cells at P3 by confocal microscopy**.** Note Venus$^+$ cells (arrowheads) are CD206^{low} (red, **f**), GFAP$^-$, Olig2$^-$, NG2$^-$ (red, **h**). **(i)** Representative example of the absence of cell proliferation (BrdU$^+$; red) in Venus$^-$ cells in the mouse postnatal hippocampus (P3). **(j)** Quantification of the apoptosis of Venus$^+$ cells in the brain (Cortex, Hippocampus and Cerebellum) at P3, analysed as expression of cleaved caspase-3 or condensation of chromatin (DAPI). A representative example of the expression of cleaved caspase-3 (red) in Venus$^+$ cells (green) is shown. **(k)** Expression of cleaved caspase-3 in NeuN$^+$ neurons at P3. Venus$^+$ cells shown in green. Scale bars in (**b, c, g, h, k**) 20μm, in (**i, j**) 100μm. Data shown in **(d, e, f, j)** represented as mean±SEM (N=6). Statistical differences: **(d)** CB *p<0.05 vs P6, CX *p<0.05 vs P21, HC *p<0.05 vs P6. **(e)**

*p<0.05 vs P0, #p<0.05 vs P3, ##p<0.01 vs P3. **(f)** **p<0.01. Data were analysed with a two-way ANOVA and a post-hoc Tukey test **(d, e)** or a t-test **(f)**.

Figure 2. The density of microglial cells remains steady through lifetime, without a significant contribution of circulating monocytes.

(a) Quantification of microglial density ($Iba1^+$ cells) across brain regions (CX, cortex; CC, corpus callosum; CA1-2, hippocampal CA1-2; DG, dentate gyrus; TH, thalamus; OB, olfactory bulb) in young (4-6 months) and aged (18-24 months) mice. **(b)** Quantification of microglial density ($Iba1^+$ cells) across brain regions (see **(a)**) in young (4-6 months) and aged (18-24 months) wild-type (WT) or $CCR2^{-/-}$ mice. **(c)** Quantification of microglial density ($Iba1^+$ cells) in the white and grey matter of the human temporal cortex, in young or aged individuals. **(d)** Representative images of Iba1 staining in human temporal cortex. **(e)** Representative example of a multinucleated microglial aggregate (c-fms EGFP) in ageing mice. **(f)** Representative examples of multinucleated microglial aggregates in ageing WT mice, absent from $CCR2^{-/-}$ mice. Scale bars in (**d, e**) 50μm, in (**f**) 50μm. Data shown in represented as mean±SEM. N=7 (**a, b**), N=15 (**c**). Statistical differences: *p<0.05. Data were analysed with a two-way ANOVA and a post-hoc Tukey test **(a, b, c)**.

Figure 3. Proliferation of microglia in the adult mouse and human brain.

(a) Analysis of the proliferation (proliferation rate, %) of microglia across brain regions (CX, cortex; CC, corpus callosum; CA1-2, hippocampal CA1-2; DG, dentate gyrus; TH, thalamus; OB, olfactory bulb) in young (4-6 months) and aged (18-24 months) mice. **(b)** Time-course analysis of microglial proliferation (proliferation rate, %) and death in the mouse cortex (CX) and dentate gyrus (DG). **(c)** Representative example of a proliferating microglial cell ($Iba1^+$, brown), incorporating BrdU (blue). **(d, e)**

Analysis of the proliferation (proliferation rate, %) of microglia in the human white or grey matter of the temporal cortex, analysed as expression of Ki67 (blue) in $Iba1^+$ cells (brown), as shown in the representative example **(e)**. **(f, g)** Analysis of microglial density ($PU.1^+$ cells) after chronic treatment with a control diet (RM1) or a diet containing a CSF1R inhibitor (GW2580). Representative staining is shown in **(g)**. **(h-j)** Analysis of microglial proliferation by tracing c-fms EGFP mice with Eco-SFFV mCherry γ-retroviral vectors (Eco-SFFV-RV)(experimental scheme shown in **h**). **(i)** Representative image of the tracing of proliferating microglia by Eco-SFFV-RV (mCherry, red) in the cortex of c-fms EGFP mice (green). **(j)** Analysis of the proliferation (proliferation rate, % $mCherry^+EGFP^+$/Total $EGFP^+$) of microglia (CX, cortex; ST, striatum) in c-fms EGFP mice. Data shown in represented as mean±SEM. N=8 (**a, b**), N=15 (**d**), N=6 (**f**), N=5 (**j**). Statistical differences: *p<0.05. Data were analysed with a two-way ANOVA and a post-hoc Tukey test **(a, b)** or a Student's T-test **(f, j)**. Scale bars in (**c**) 20μm, in (**e**) 50μm, in (**g**) 100μm.

(k-n) Analysis of microglial proliferation by 2-photon imaging of $CX_3CR1^{GFP/+}$ mice. **(k)** Maximal intensity projection (MIP) images of the same field of view (142 - 153 μm depth, step 1 μm) in a $CX_3CR1^{GFP/+}$ mouse taken at different time points as indicated (see timestamps, relative time). Arrows point to a proliferating microglial cell and to its progeny. **(l)** Proliferation rate of microglia (median ± interquartile range, IQR; n=669 cells, 9 fields of view (FOV), 4 mice). **(m)** Mean distance between the centers of two neighboring cells for resident cells and for newborn cells during the first 24 hours of their life (mean ± SEM; n= 62 cells, 9 FOVs, 4 mice). **(n)** Distance between the twin microglial cells as a function of their age (median ± IQR; n= 31 pair of twin cells, 8 FOVs, 4 mice). Statistical differences: **(m)** *p<0.001, Student's T-Test. Scale bar in (**a**) 20μm.

Figure 4. The homeostatic turnover of microglia is not maintained by Nestin$^+$ precursors

(a-c) Immunofluorescent detection and confocal analysis of Iba1$^+$ microglia (red) in nestin-EGFP (green) mice, in the cortex (**a, c**) or hippocampal dentate gyrus (**b**). (**d**) Triple immunofluorescence for BrdU (blue), Iba1$^+$ (microglia, red) and nestin-EGFP (green) in the dentate gyrus. Open arrowhead indicates a BrdU$^+$Iba1$^-$Nestin$^+$ cell, while white arrowhead indicates a BrdU$^+$Iba1$^+$Nestin$^-$ cell. Scale bar in (**a, b**) 50μm, (**c, d**) 20μm. N=5.

Figure 5. The turnover of microglia is balanced by apoptosis

(a) Maximal intensity projection (MIP) images of the same field of view (88 - 106 μm depth, step 2 μm) in a $CX_3CR1^{GFP/+}$ mouse. Arrows point to a disappearing (i.e. dying) microglial cell. **(b)** Death rate of microglia (median ± IQR; n= 669 cells, 9 FOVs, 4 mice). **(c)** Microglial density across regions (CX, cortex; CC, corpus callosum; CA1-2, hippocampal CA1-2; DG, dentate gyrus; TH, thalamus) in wild-type (WT), PUMA$^{-/-}$, BIM$^{-/-}$ and Vav-Bcl2 mice. **(d)** Expression of Vav (red) in microglia (c-fms EGFP, green), analysed by confocal microscopy. **(e)** Time-course analysis of postnatal (P0-P231) microglial density in wild-type (WT) and Vav-Bcl2 mice. **(f)** Representative example of microglial cells (Iba1$^+$) in the cortex of WT and Vav-Bcl2 mice. Data shown in (**c, e**) represented as mean±SEM. N=4, 3, 4, 7 (**c;** WT, PUMA$^{-/-}$, BIM$^{-/-}$ and Vav-Bcl2 mice, respectively), N=4 (**e**). Statistical differences: *p<0.05, **p<0.01, ***p<0.001. Data were analysed with a two-way ANOVA and a post-hoc Tukey test **(c, e)**. Scale bars in (**a, d**) 20μm, in (**f**) 100μm.

Figure 6. Transcriptomic profiling of microglia from WT and Vav Bcl-2 mice

(a) Flow cytometry analysis and sorting (FACS) of microglia from WT and Vav Bcl-2 mice. Crosshair in FACS plots shows gating parameters used to define $CD11b^{+}CD45^{low}$ and $CD11b^{+}CD45^{high}$ subpopulations and subsequent sorting. Statistical differences: ****p<0.0001. Data were analysed with a t-test **(a)**. **(b)** Heatmap representation of genes showing a significant (*P* <0.01; >10-fold change) change in Vav Bcl-2 vs WT microglia (combined $CD45^{+}$). Clustering of genes by expression profiles is shown on the left. **(c)** Clustered representation (GOslim) of GO processes significantly altered in Vav Bcl-2 compared to WT microglia. Number of genes altered per cluster is shown on top of bars. **(d)** Enrichment map of GO terms, where red nodes represent GO terms and green edges represent shared genes (thicker lines indicate more shared genes).**(e)** Venn diagram representing the intersection of the transcriptional variability observed when comparing total (blue), $CD45^{low}$ (green) or $CD45^{high}$ (yellow) Vav Blc-2 to WT microglia.

Figure 7. Temporal and spatial coupling of microglial proliferation and death.

(a) MIP images of a sample field of view (50-80 µm depth, step 1 µm) in a $CX_3CR1^{GFP/+}$ mouse taken at the beginning (left, day 0) and at the end (right, day 22) of the imaging period. Note that bone growth occurred in the lower right corner of the latter image. **(b)** 3D matrix illustrating the history of cells in the sample field of view (317 µm x 317 µm x 160 µm) during the 22-day-long imaging period. Stable cells are shown in grey, cells, which are going to die, are shown in red and cells going to divide are shown in blue. This FOV includes the cells shown in **(a)**. **(c)** Temporal relationship between death and proliferation events (n= 68 cells, 9 FOVs, 4 mice). The time when a cell dies is set as day 0 (reference point) and the relative time when proliferation occurs in its vicinity (≤ 200 µm) is calculated. The pie chart illustrates the

fractions of cells, proliferating in the vicinity of a dying cell 4 days before (light grey), during (grey) or 4 days after (dark grey) the death of the reference cell. **(d)** Spatial relationship between a dead cell and the nearest proliferating or resident cell (n= 53 dead cells, 9 FOVs, 4 mice). **(e)** Summary of the data shown in **(d)** (median ± IQR; n= 53 cells, 9 FOVs, 4 mice). Statistical differences: *p<0.001, Wilcoxon signed-ranks test. Scale bar in (**a**) 50μm.

Askew et al. Fig. 1

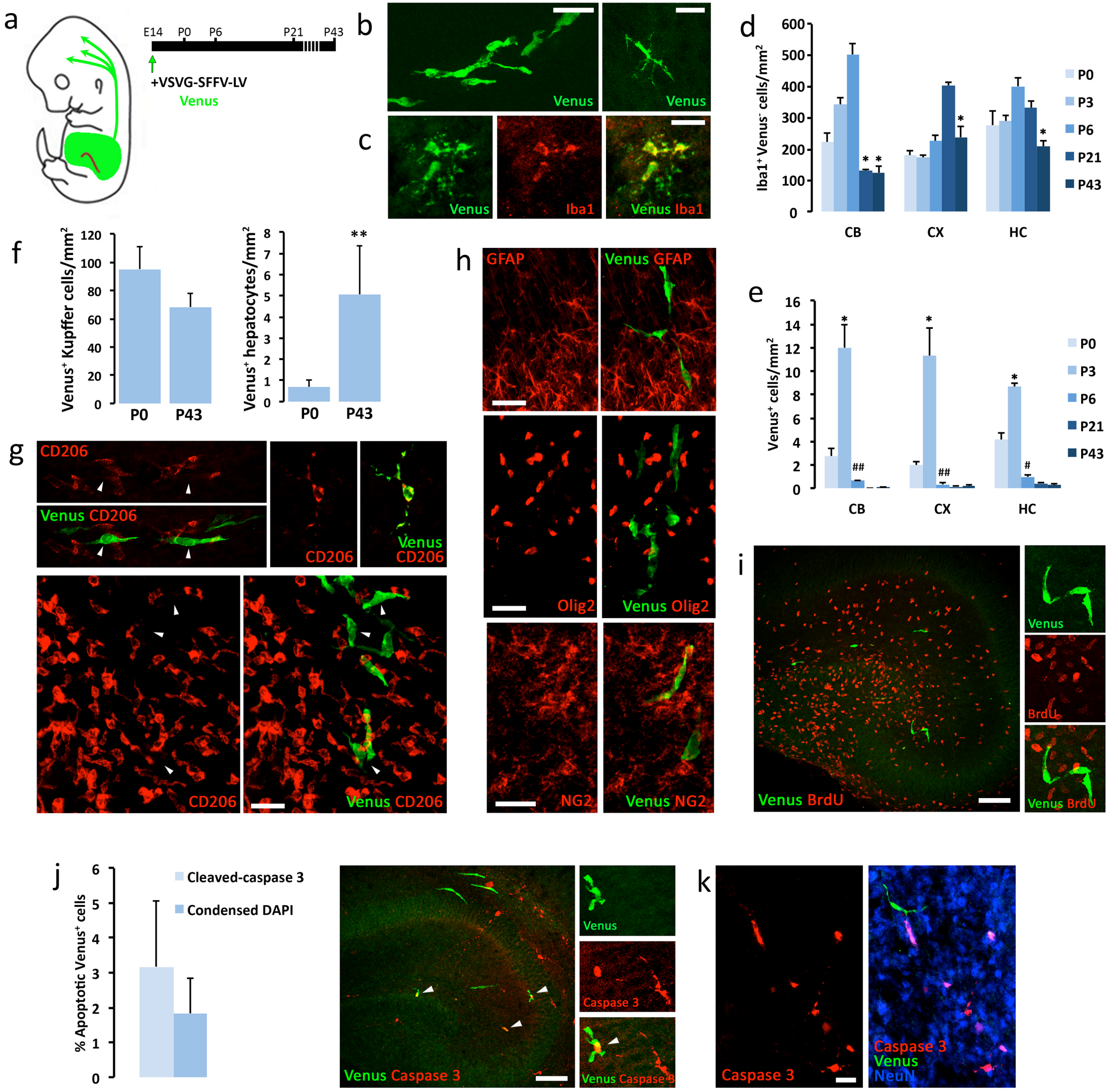

Askew et al. Fig. 2

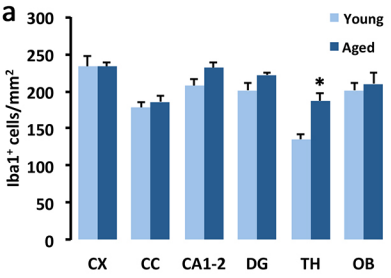

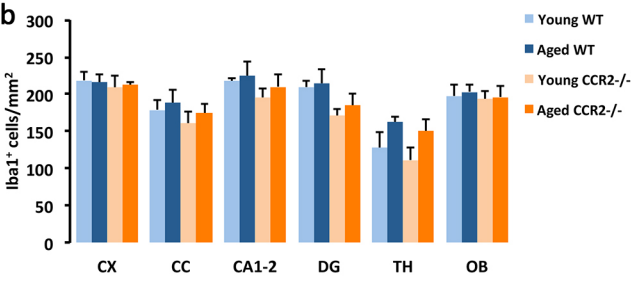

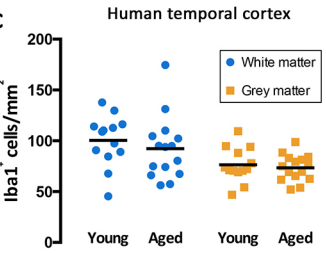

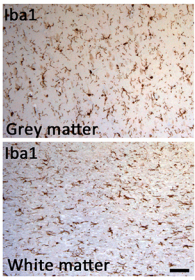

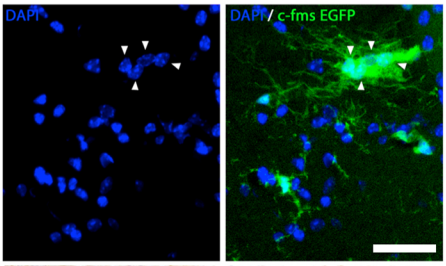

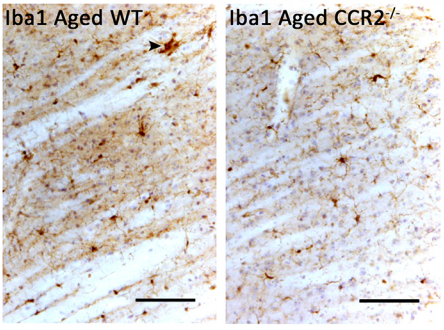

Askew et al. Fig. 3

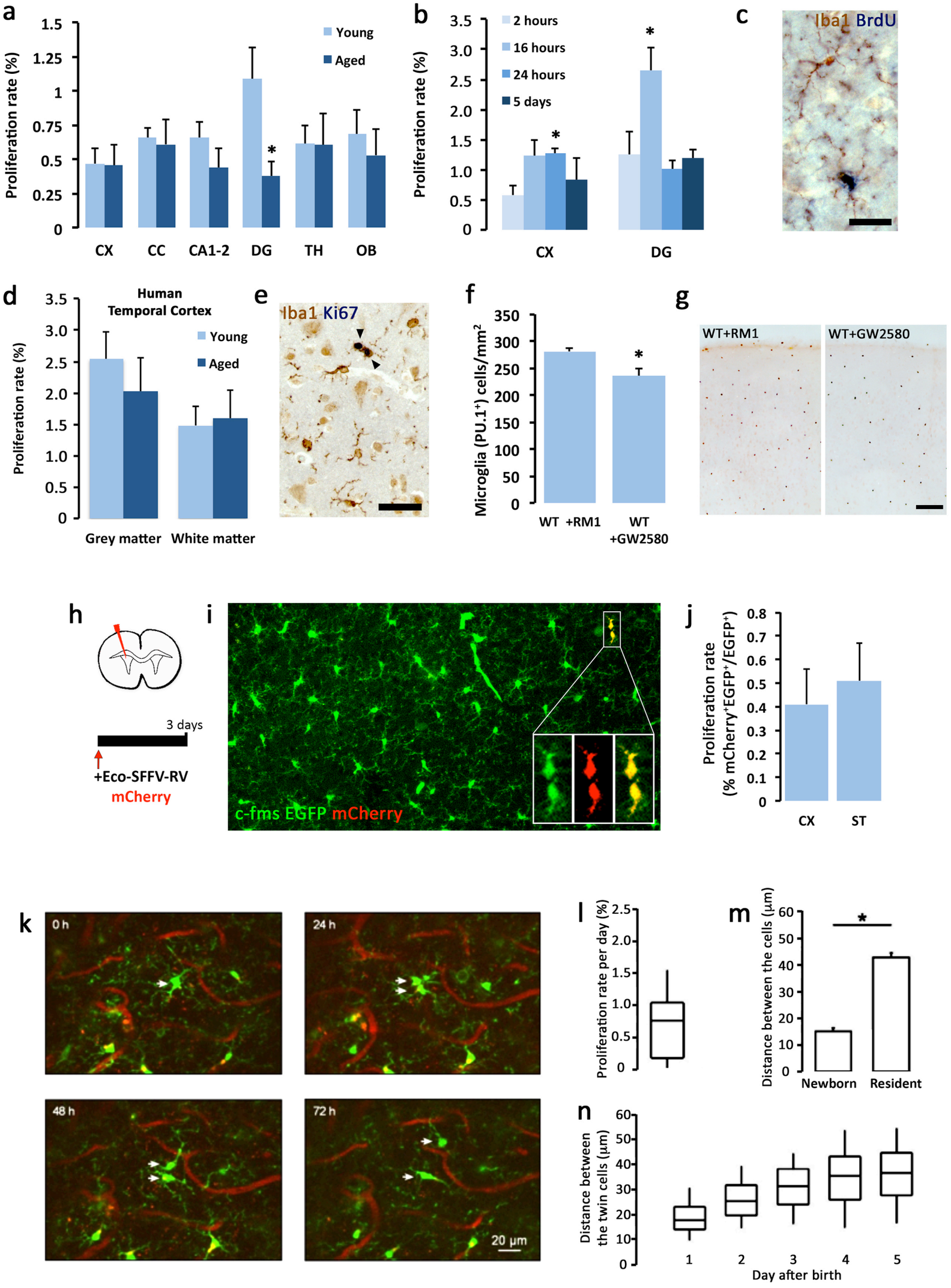

Askew et al. Fig. 4

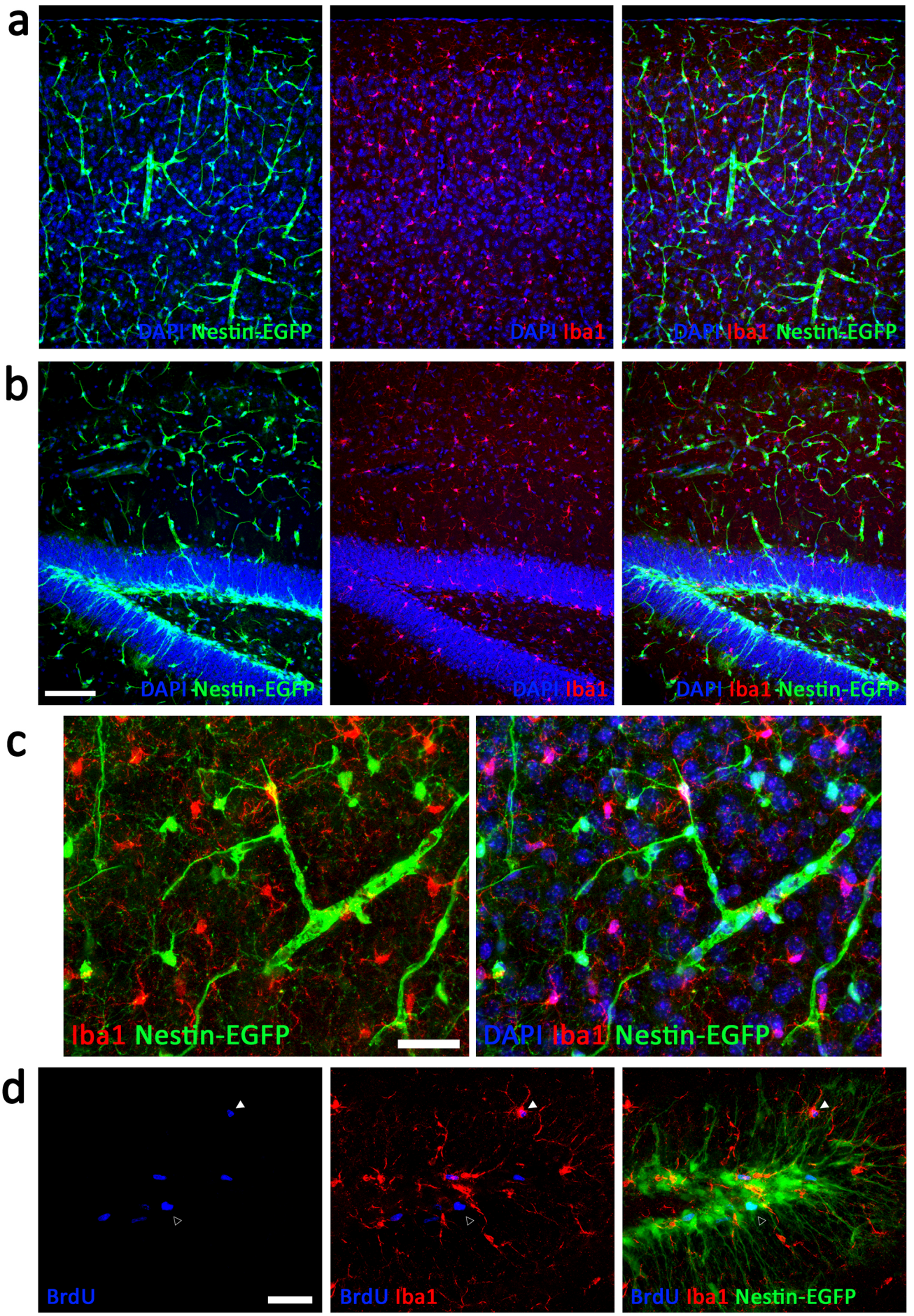

Askew et al. Fig. 5

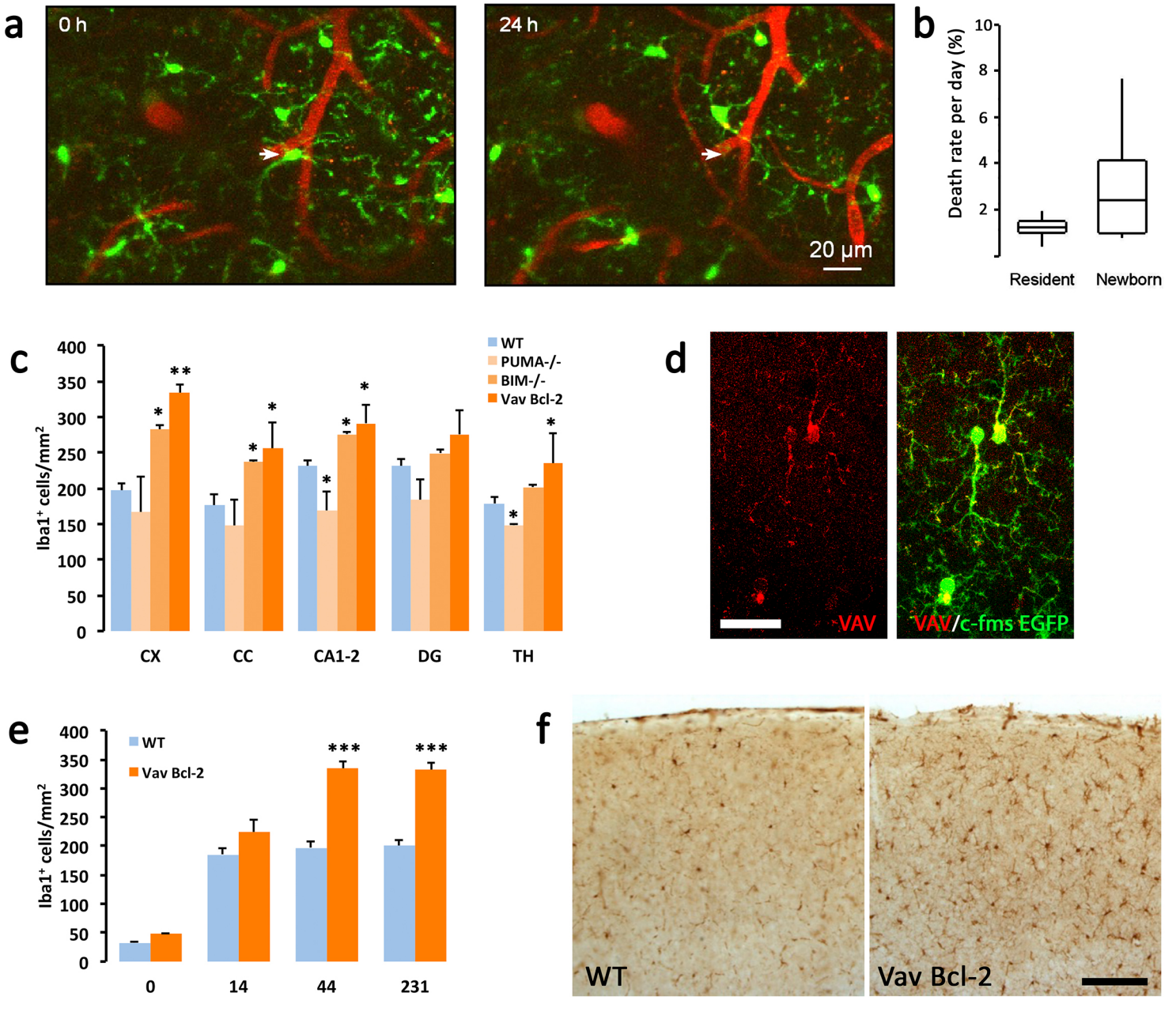

Askew et al. Fig. 6

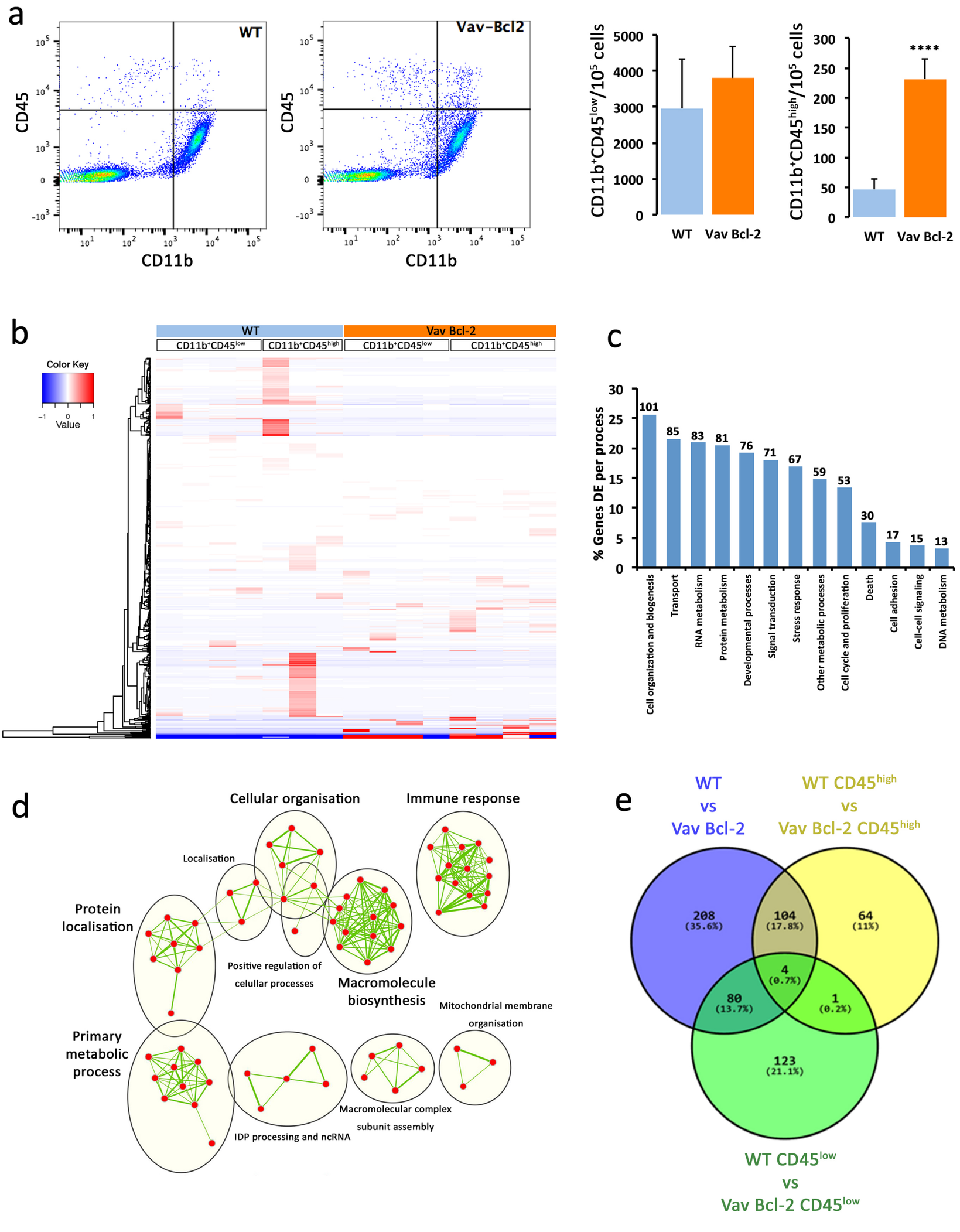

Askew et al. Fig. 7